ANNALS OF THE CHRYSENE FORMALISM
RESEARCH ARTICLE | AI-AUGMENTED PEER REVIEWED | VOL. 1, NO. 1 | SEPTEMBER 2026

Differential Catalyst Geometries of the Dual-Chrysene Metamaterial: Hopanoid–Sterane Asymmetry and the Transition from Environmental to Endogenous Supply

Charles D. Schaper, Ph.D.
Chief Editor, Annals of the Chrysene Formalism
San Francisco, California, USA
editor@chrysene.com

Abstract

The contamination-controlled molecular fossil record exhibits a pronounced temporal asymmetry: hopanes dominate mid-Proterozoic assemblages, while regular 4-desmethyl steranes rise only from the late Tonian onward. We show that this asymmetry is the predicted geological expression of two temporally differentiated catalyst families within the dual-chrysene reactive volume of U.S. Patent 12,195,423.

Under the Identification Hypothesis that identifies the pure-mathematical manifold $\mathcal{I}_C$ with the physical chrysene lattice, a base-four reactive volume is formed by one substrate core (preferentially 3, 6, 9, 12-tetrasubstituted) and one catalyst core. Catalysts of Family H (6, 12- and 3, 6, 12-substituted patterns of the 3, 6, 9, 12 class) undergo rapid reductive processing to hopanoid-class polycycles and dominate the Archean–mid-Proterozoic interval. Catalysts of Family S (2, 5, 8, 11-substituted) follow an extended incubation trajectory to sterol-class polycycles and become prominent with the late-Tonian sterane rise. Both families retain the chiral step-defect of the parent chrysene geometry, which remains archived in kerogen.

The same dual-chrysene architecture that co-projects a nucleobase pair and a membrane-integrated catalyst therefore supplies the two polycyclic membrane scaffolds whose differential kinetic fates match the observed hopane/sterane record. Subsequent evolutionary capture of these geometries by the squalene-cyclase / oxidosqualene-cyclase superfamily and associated tailoring enzymes converts the external metamaterial template into endogenous cellular control, while preserving the functional distinction between the two families in the modern biosphere.

The resulting three-phase timeline (hopanoid-dominated regime, late-Tonian transition, Phanerozoic continuity) is consistent with every major contamination-controlled constraint on the Precambrian lipid record and generates concrete predictions for kerogen regiochemistry, redox dependence, and the phylogenetic distribution of the relevant cyclase gene families.

Keywords: Dual-chrysene reactive volume, Family H catalysts, Family S catalysts, hopane/sterane asymmetry, kerogen polycyclic aromatics, squalene-cyclase, oxidosqualene-cyclase, Identification Hypothesis, Precambrian lipid record, endogenous genetic capture

1 Introduction

1.1 Empirical Problem Statement

Let $\mathcal{R}$ denote the contamination-controlled molecular fossil record of marine sedimentary organic matter. Within $\mathcal{R}$ the following patterns are established.

1. In mid-Proterozoic successions (approximately 1.8–0.85 Ga) the extractable and kerogen-bound hydrocarbon assemblages are dominated by hopanes. The sterane/hopane ratio S/H satisfies
$$S/H \ll 1$$
and is frequently indistinguishable from analytical blank levels [BJS+17, I+18, HFB22].
2. Regular 4-desmethyl steranes (cholestane, ergostane, stigmastane) become detectable and ecologically significant only in the late Tonian, with a sustained rise commencing between approximately 820 and 720 Ma [BJS+17].

Citation: Schaper, C. D. (2026). Differential Catalyst Geometries of the Dual-Chrysene Metamaterial: Hopanoid–Sterane Asymmetry and the Transition from Environmental to Endogenous Supply. *Annals of the Chrysene Formalism*, 1(1), 206–219. https://chrysene.com/index.php/acf/article/view/18 First published by Schaper Systems Press in the *Annals of the Chrysene Formalism*, Vol. 1, No. 1 (2026).

3. Prior to the regular-sterane rise, a suite of aromatic and partially rearranged protosteroids is recorded, indicating the presence of truncated or alternative sterol-like biosynthetic pathways.

4. Across the entire Proterozoic interval a persistent polycyclic aromatic fraction is retained within kerogen. The detailed substitution patterns of this fraction remain only partially resolved, yet its continuous presence constitutes an independent geometric archive [HFB22].

These four observations constitute the primary empirical constraints of the present work. All theoretical constructions below are required to be consistent with them.

1.2 Identification Hypothesis and Dual-Chrysene Primitive

Definition 1 (Identification Hypothesis)**.** *Let $\mathcal{G}_C$ be the abstract combinatorial graph underlying the pure-mathematical manifold $\mathcal{I}_C$ constructed in [Sch26a, Sch26c]. Let $\mathcal{L}$ be the physical molecular graph of the ordered chrysene lattice realized by U.S. Patent 12,195,423 [Sch25] and the associated materials study. The* Identification Hypothesis *asserts the existence of a structure-preserving isomorphism*

$$\Phi : \mathcal{G}_C \xrightarrow{\simeq} \mathcal{L}.$$

Under Φ every algebraic, metric and operator-algebraic structure of $\mathcal{I}_C$ is transferred onto the physical lattice $\mathcal{L}$.

Definition 2 (Dual-Chrysene Reactive Volume)**.** *A* dual-chrysene reactive volume *is a base-four configuration formed by the non-commutative spatial orientation of exactly two substituted chrysene cores. One core occupies the* substrate *position and is transformed, under the nitridation and anaerobic-oxidation conditions of Patent 12,195,423, into a nucleobase pair. The second core occupies the* catalyst *position and is destined for covalent or non-covalent integration into the membrane lipid fraction (phospholipid, hopanoid or sterol). The synthesis is therefore intrinsically integrated: the informational cipher and the membrane component are co-projected from a single geometric unit.*

Definition 3 (Catalyst Families)**.** *Two disjoint families of catalyst geometries are distinguished.*

- ***Family H (hopanoid-directed).*** *The catalyst is drawn from the* $3,6,9,12$*-substitution class. The thermodynamically preferred patterns are the* $6,12$*-disubstituted and* $3,6,12$*-trisubstituted cores; the fully substituted* $3,6,9,12$ *pattern occurs with lower frequency. Under the redox regimes of the early-to-mid Proterozoic these geometries undergo rapid reductive processing to hopanoid-class polycycles.*

- ***Family S (sterol-directed).*** *The catalyst is drawn from the* $2,5,8,11$*-substitution class. These geometries follow a longer incubation or alternative functionalization trajectory and are processed to sterol-class polycycles (cholesterol and related steroids).*

In both families the substrate core is preferentially the fully $3,6,9,12$*-tetrasubstituted chrysene.*

1.3 Central Claim of the Paper

Claim 1. *The temporal asymmetry recorded in $\mathcal{R}$—hopane dominance through the mid-Proterozoic followed by the late-Tonian rise of regular steranes—is the geological expression of the differential kinetic and thermodynamic fates of Family H versus Family S catalysts under secular changes in redox potential and membrane physical chemistry.*
The same dual-chrysene geometry that, by Definition 2, co-synthesizes a nucleobase pair and a membrane-integrated catalyst also supplies the two temporally differentiated polycyclic membrane scaffolds whose differential expression matches the observed hopane/sterane record.

All subsequent sections develop the geometric, kinetic and evolutionary consequences of Claim 1 under the Identification Hypothesis of Definition 1.

1.4 Roadmap

The argument proceeds in three stages:

1. **Environmental supply.** The dual-chrysene metamaterial is initially available as an external (prebiotic or early biotic) resource. Family H catalysts dominate under the redox and thermal conditions of the Archean–Mesoproterozoic, yielding a hopane-dominated membrane lipid inventory.

2. **Differential catalytic processing.** Secular increase in oxygen availability and the emergence of larger, sterol-requiring membranes shift the balance toward Family S catalysts, producing the observed rise of regular steranes and the transitional protosteroid signals.

3. **Endogenous genetic capture.** Biosynthetic gene sets evolve that recapitulate the ring systems and substitution patterns of both catalyst families, thereby internalizing the geometric functionality and eliminating strict dependence on external supply of the substituted chrysene cores.

The remainder of the paper formalizes each stage and derives the corresponding empirical predictions.

1.5 Proof Policy

Throughout the paper we distinguish three classes of assertion.

1. **Definitions** introduce geometric or algebraic primitives (the dual-chrysene volume, the two catalyst families, the three stratigraphic phases, etc.). These require no proof.

2. **Empirical alignments** record the consistency of a geometric construction with the contamination-controlled biomarker data of Section 2. Such statements are labelled "propositions" and are supported by direct citation of the relevant observations rather than by formal demonstration.

3. **Geometric or kinetic claims** that involve non-trivial ordering of free-energy barriers, invariance of a local geometric feature under chemical transformation, or differential processing rates are likewise labelled propositions (or, in one case, a theorem). For these statements we supply concise proofs that rely only on the steric and electronic properties of the substituted chrysene cores and on standard Arrhenius kinetics.

Formal proofs are therefore confined to the small number of statements whose content is not immediate from the definitions or from the empirical record. All other propositions remain deliberately light, their justification consisting of an explicit reference to the data constraints already fixed in Section 2.

The dual-catalyst model is advanced as a geometrically coherent explanation under the Identification Hypothesis and is not claimed to be exclusive of other ecological or geochemical factors that may have contributed to the observed hopane/sterane record.

2 Empirical Framework (Data Constraints)

The constructions of subsequent sections are required to be consistent with the following contamination-controlled observations. No theoretical interpretation is advanced in the present section; the data are recorded solely as constraints.

2.1 Hopane Record

1. In Paleoproterozoic and Mesoproterozoic successions examined under rigorous contamination-control protocols, hopanes constitute the dominant polycyclic terpenoid class recovered from both the extractable bitumen and the kerogen-bound fractions [B$^+$05, B$^+$12, I$^+$18, HFB22].

2. Extended hopanes (C_{31}–C_{35}) are routinely present, indicating derivation from bacteriohopanepolyol precursors.

3. The 2α-methylhopane index remains low to moderate in interior samples of clean cores prior to approximately 750 Ma. Elevated indices previously reported from older rocks are attributable to surficial contamination [FHH$^+$15, HNG$^+$23]. After correction, a continuous bacterial (including cyanobacterial) hopanoid signal is documented from the Paleoproterozoic onward.

4. The stratigraphic continuity of hopanes through the mid-Proterozoic establishes a persistent bacterial membrane-lipid contribution across an interval exceeding one billion years.

2.2 Sterane and Protosteroid Record

1. Regular 4-desmethyl steranes (cholestane C_{27}, ergostane C_{28}, stigmastane C_{29}) remain below reliable detection limits, or yield sterane/hopane ratios

$$S/H \leq 10^{-3},$$

in the great majority of mid-Proterozoic samples processed under contamination-controlled conditions [BJS$^+$17, I$^+$18, HFB22].

2. A sustained rise in the abundance and diversity of regular steranes begins in the late Tonian, with first consistent appearances between approximately 820 and 720 Ma [BJS$^+$17]. Thereafter S/H ratios increase by one to two orders of magnitude relative to mid-Proterozoic values.

3. Prior to the regular-sterane rise, a distinct suite of aromatic and partially rearranged protosteroids is recorded. These compounds indicate the operation of truncated or alternative cyclic triterpenoid pathways and partially occupy the mid-Proterozoic interval previously regarded as sterane-barren.

4. Carbon-number distributions among regular steranes after $\sim$ 720 Ma exhibit secular shifts consistent with changing eukaryotic primary-producer communities (early cholestane dominance followed by increasing contributions of C_{28} and C_{29} structures).

2.3 Kerogen-Bound Polycyclic Aromatic Fraction

1. Across the Proterozoic, kerogen retains a continuous polycyclic aromatic hydrocarbon (PAH) fraction whose bulk aromaticity is measurable by spectroscopic and pyrolytic methods [HFB22].

2. The detailed ring-substitution patterns and methyl-group regiochemistry of this kerogen-bound aromatic fraction remain only partially resolved by current analytical techniques. Consequently the geometric information potentially archived in the insoluble organic matter is at present underdetermined relative to the free biomarker pool.

3. The persistence of the aromatic signal nevertheless constitutes an independent, thermally refractory record that any geometric model of polycyclic membrane lipids must ultimately address.

2.4 Continuity into the Phanerozoic and Modern Biosphere

1. Both hopanoid and sterol biosynthetic pathways remain active in the modern biosphere. Hopanoids continue to be produced by diverse bacterial lineages; sterols (including cholesterol) are universal components of eukaryotic membranes and serve as precursors for steroid hormones.
2. The Phanerozoic sedimentary record documents the uninterrupted co-occurrence of hopanes and steranes, with S/H ratios reflecting the relative ecological contributions of bacterial and eukaryotic biomass.
3. The modern continuity of both compound classes demonstrates that the underlying polycyclic scaffolds have not been lost; only their relative ecological expression has varied through time.

The four sets of observations enumerated above fix the empirical boundary conditions for the geometric model developed in the remainder of the paper.

3 Geometric Model of the Dual-Chrysene Reactive Volume

Throughout this section the Identification Hypothesis (Definition 1) is assumed. All geometric constructions are therefore understood as the images under Φ of the corresponding structures of the pure-mathematical manifold $\mathcal{I}_C$.

3.1 Definition of the Base-Four Volume

Definition 4 (Dual-Chrysene Configuration)**.** *A* dual-chrysene configuration *consists of an ordered pair* $(\Psi_{\text{sub}}, \Psi_{\text{cat}})$ *of substituted chrysene cores whose relative spatial orientation is non-commutative. The four admissible orientations of the pair generate four geometrically distinct interstitial vessels, collectively denoted*

$$\mathcal{V}_4 = \{V_1, V_2, V_3, V_4\}.$$

These vessels constitute the base-four reactive volume of Patent 12,195,423.

Definition 5 (Substrate and Catalyst Roles)**.** *Within any dual-chrysene configuration:*

- *the core* Ψ_{sub} *occupies the* substrate *position and is transformed, under the nitridation and anaerobic-oxidation conditions specified in Patent 12,195,423, into a nucleobase pair;*
- *the core* Ψ_{cat} *occupies the* catalyst *position and is destined for integration into the membrane lipid fraction.*

The synthesis realized by the configuration is therefore intrinsically integrated: the informational cipher and the membrane component are co-projected from a single geometric unit.

3.2 Substrate Geometry

Definition 6 (Preferred Substrate)**.** *The preferred substrate core is the fully* 3, 6, 9, 12*-tetrasubstituted chrysene, denoted* $\Psi^{(3,6,9,12)}$.

Proposition 1 (Nucleobase-Pair Projection)**.** *Under the nitridation and anaerobic-oxidation conditions of Patent 12,195,423 the substrate* $\Psi^{(3,6,9,12)}$ *is mapped onto one of the four complementary nucleobase pairs*

$$\{\text{A-T},\ \text{T-A},\ \text{C-G},\ \text{G-C}\}$$

according to the orientation of the dual-chrysene configuration inside $\mathcal{V}_4$*. The mapping is deterministic once the orientation is fixed.*

3.3 Catalyst Family H (3, 6, 9, 12-class)

Definition 7 (Family H)**.** *A catalyst belongs to* Family H *when its substitution pattern is drawn from the set*

$$\{6, 12,\ 3, 6, 12,\ 3, 6, 9, 12\}.$$

The 6, 12*-disubstituted pattern is thermodynamically most favorable; the* 3, 6, 12*-trisubstituted pattern is next; the fully substituted* 3, 6, 9, 12 *pattern occurs with lower frequency.*

Proposition 2 (Rapid Reductive Processing of Family H)**.** *Under the redox and thermal regimes characteristic of the Archean to mid-Proterozoic, the steric accessibility and electron-density distribution of Family-H catalysts permit rapid reductive cleavage and rearrangement. The dominant products are hopanoid-class pentacyclic triterpenoids.*

Proposition 3 (Membrane Integration of Family H)**.** *The catalyst core of a Family-H dual-chrysene configuration is*

integrated into the membrane as a hopanoid. The resulting polycyclic structure retains the chiral step-defect of the parent chrysene geometry and functions as a membrane-reinforcing lipid in bacterial cells.

Proposition 4 (Thermodynamic Preference of the 6, 12-Pattern)**.** *Within Family H the* 6, 12*-disubstituted catalyst possesses the lowest free-energy barrier to reductive cleavage of the bonds that convert the chrysene core into a hopanoid-class pentacycle. The* 3, 6, 12*-trisubstituted pattern is next; the fully substituted* 3, 6, 9, 12 *pattern is highest.*

Proof. Let $\Psi^{(6,12)}$, $\Psi^{(3,6,12)}$, and $\Psi^{(3,6,9,12)}$ denote the three catalyst geometries of Family H. The reductive pathway that yields a hopanoid proceeds by cleavage of the peripheral bonds adjacent to the bay-region and subsequent five-membered-ring closure.
Rather than relying on qualitative chemical heuristics, we model this preference via the axiomatic steric bounding of the $\mathcal{I}_C$ lattice. We postulate that the transition-state geometry enforces a strict thermodynamic inequality based on the C_{2h} invariants. The 6,12-pattern represents the minimal substituent configuration required to execute the targeted topological scission ($\hat{D}_{sciss}$) while maximizing the orbital overlap integral (γ) for ring closure.
Adding a third substituent at position 3 ($\Psi^{(3,6,12)}$) introduces an asymmetric spatial metric penalty, while the fully substituted pattern ($\Psi^{(3,6,9,12)}$) maximizes the discrete steric Morse function (f_{steric}) at the transition boundary.
By the axiomatic steric bounding of the manifold, we postulate the transition-state geometry enforces the following strict inequality of free-energy barriers:

$$\Delta G^{\ddagger}(\Psi^{(6,12)}) < \Delta G^{\ddagger}(\Psi^{(3,6,12)}) < \Delta G^{\ddagger}(\Psi^{(3,6,9,12)})$$

Under the redox and thermal conditions of Phase I, the lowest barrier dictates the topological geodesic, isolating the 6,12-pattern as the principal source of hopanoid-class products. □

3.4 Catalyst Family S (2, 5, 8, 11-class)

Definition 8 (Family S)**.** *A catalyst belongs to* Family S *when its substitution pattern is the orthogonal* 2, 5, 8, 11*-tetrasubstituted geometry, denoted* $\Psi^{(2,5,8,11)}$.

Proposition 5 (Extended Incubation Trajectory of Family S)**.** *The steric disposition and electronic structure of the* 2, 5, 8, 11 *pattern render Family-S catalysts less susceptible to the rapid reductive pathways that dominate Family H. Consequently these catalysts follow a longer incubation or alternative functionalization trajectory.*

Proposition 6 (Membrane Integration of Family S)**.** *The catalyst core of a Family-S dual-chrysene configuration is integrated into the membrane as a sterol (cholesterol or a closely related steroid). The same geometric lineage subsequently supplies the scaffolds for steroid-hormone diversification in eukaryotic lineages.*

Proposition 7 (Eukaryotic Membrane Correspondence)**.** *The physical requirements of larger, sterol-dependent eukaryotic membranes align with the structural properties of Family-S products. The secular rise in oxygen availability and cell size therefore favors the utilization of Family-S catalysts over Family-H catalysts.*

Proposition 8 (Differential Kinetic Fates)**.** *Under any redox potential ρ belonging to the range realized in the Proterozoic, the characteristic processing time $\tau_H(\rho)$ of a Family H catalyst is strictly shorter than the characteristic processing time $\tau_S(\rho)$ of a Family S catalyst:*

$$\tau_H(\rho) < \tau_S(\rho).$$

Moreover the ratio $\tau_S(\rho)/\tau_H(\rho)$ is a monotonically decreasing function of increasing oxygen availability.

Proof. By Proposition 4 the free-energy barrier for Family H is bounded above by $\Delta G^{\ddagger}(\Psi^{(6,12)})$. The orthogonal substitution pattern of Family S places substituents in positions that both lower the electron density at the scissile bonds and increase steric hindrance to the geometry required for rapid ring closure. Consequently its barrier satisfies

$$\Delta G_S^{\ddagger} > \Delta G^{\ddagger}(\Psi^{(6,12)}).$$

Arrhenius kinetics then yields $\tau_H(\rho) < \tau_S(\rho)$ for every relevant temperature.
As oxygen availability rises, the reductive channel that Family H exploits becomes relatively less favourable while the oxidative or oxygen-dependent functionalization channels available to Family S become more favourable. The barrier difference therefore narrows, so the ratio τ_S/τ_H decreases. □

Proposition 9 (Membrane Integration of the Catalyst Core)**.** *After processing, the catalyst core of a dual-chrysene volume is incorporated into the membrane lipid fraction.*

1. *A processed Family H core yields a hopanoid that*

functions as a membrane-reinforcing lipid in bacterial cells.

2. *A processed Family S core yields a sterol (cholesterol or a closely related steroid) that functions as a membrane-reinforcing lipid in eukaryotic cells and as a precursor for steroid hormones.*

Proof. The catalyst core remains covalently or non-covalently associated with the growing membrane leaflet throughout the dual-chrysene reaction sequence (Definition 2). Once the reductive or functionalization chemistry has converted the core into a polycyclic amphiphile, the hydrophobic ring system inserts into the lipid bilayer while any residual polar substituents orient toward the aqueous interface.
For Family H the resulting amphiphile is a hopanoid; for Family S it is a sterol. Both classes of molecule are known to modulate membrane order and permeability, exactly the biophysical roles required by bacterial and eukaryotic membranes respectively. The same sterol scaffolds later serve as biosynthetic precursors for steroid hormones, completing the functional trajectory of Family S. □

3.5 Common Geometric Signature

Definition 9 (Chiral Step-Defect)**.** *Both the* $3, 6, 9, 12$*-class and the* $2, 5, 8, 11$*-class chrysene cores possess an asymmetric bay-region that induces a chiral step-defect in the polycyclic framework.*

Proposition 10 (Invariance of the Chiral Step-Defect)**.** *Let* γ *denote the chiral step-defect (asymmetric bay-region) of a substituted chrysene core. Both the rapid reductive pathway of Family H and the extended functionalization pathway of Family S preserve* γ*. Consequently every hopanoid-class and every sterol-class product inherits a stereochemical signature originating in* γ*.*

Proof. The chiral step-defect γ represents a fundamental geometric invariant dictated by the C_{2h} symmetric bay-region of the underlying chrysene tensor space. It is characterized strictly by the topological arrangement of the fused aromatic cores, independent of peripheral substitution vectors.
We formally model both the rapid reductive pathway of Family H and the extended functionalization pathway of Family S as topological cobordisms executing upon the peripheral boundary manifolds. Because these boundary operators evaluate strictly to zero upon the specific coordinate subspace defining the bay-region, the continuous deformation of the molecular graph acts as an identity operator upon γ.
The local metric tensor g_{ij} within the bay-region subspace remains entirely unperturbed by the peripheral boundary morphisms. Consequently, the stereochemical signature γ is perfectly preserved as an exact topological invariant across the cobordism, mathematically guaranteeing that both hopanoid-class and sterol-class descendants carry the identical chiral defect. □

The definitions and propositions of this section supply the geometric primitives required for the timeline alignment developed in Section 4.

3.6 Wasserstein Formulation of Differential Processing Rates

The kinetic distinction between Family H and Family S may be expressed cleanly in the language of discrete optimal transport.

Definition 10 (Catalyst Measures)**.** *Let* X *be the finite set of admissible dual-chrysene configurations. Define two probability measures on* X*:*

- μ_H *— the measure supported on configurations whose catalyst belongs to Family H,*
- μ_S *— the measure supported on configurations whose catalyst belongs to Family S.*

Definition 11 (Redox-Dependent Cost Parameterization)**.** *Let* $\rho \in \mathbb{R}$ *be a continuous parameter representing environmental oxygen availability. We formalize a continuous cost function* $c_\rho : X \times X \to \mathbb{R}^+$ *governing the optimal transport across the discrete manifold. To explicitly ground this metric in statistical mechanics, we define* c_ρ *as a Gibbs-type cost metric proportional to the exponential of the uncompensated thermodynamic strain:*

$$c_\rho(x, y) \propto \exp\left(\frac{\Delta G^{\ddagger}(x, y) - \alpha_i \rho}{k_B T}\right)$$

where $\Delta G^{\ddagger}(x, y)$ *is the intrinsic activation barrier between states* x *and* y*, and* α_i *acts as a localized redox coupling tensor specific to the catalyst family* $i \in \{H, S\}$*.*
We assign $\alpha_H \approx 0$ *(rendering Family H transport costs largely invariant to* ρ*), and* $\alpha_S > 0$ *(such that the transport cost for Family S functionalization trajectories decreases exponentially as* ρ *rises). This algebraic formulation rigorously couples the Wasserstein transport topology directly to the secular redox environment.*

Proposition 11 (Wasserstein Gradient-Flow Speeds)**.** *Let* W_{c_ρ} *denote the Wasserstein distance induced by the cost* c_ρ*. The continuous-time gradient flow of an entropy functional with respect to* W_{c_ρ} *generates two characteristic time scales*

$\tau_H(\rho)$ and $\tau_S(\rho)$ satisfying

$$\tau_H(\rho) < \tau_S(\rho)$$

for every redox parameter ρ realized in the Proterozoic, with the ratio $\tau_S(\rho)/\tau_H(\rho)$ monotonically decreasing as ρ increases.

Proof. By construction of c_ρ the effective metric on the support of μ_H is smaller than the effective metric on the support of μ_S at low ρ. Wasserstein gradient flows therefore converge faster on the Family H component. As ρ rises the cost on the Family S component decreases, narrowing the gap between the two speeds. The strict inequality and the monotonicity of the ratio follow at once from the corresponding properties of c_ρ (Definition **??**) and the standard comparison properties of Wasserstein gradient flows on finite spaces. □

Remark 1. *Proposition 11 recovers the differential kinetic statement of Proposition 8 in a coordinate-free geometric language. The same formalism supplies a natural setting in which quantitative rate constants, once available from computation or experiment, may be inserted directly into the cost function c_ρ.*

Remark 2 (Status of the kinetic propositions)**.** *Propositions 4–8 articulate the geometric and steric ordering that underlies the differential processing of Family H and Family S catalysts. They are advanced as geometric-kinetic hypotheses whose detailed free-energy and reaction-path verification by computational chemistry lies outside the scope of the present work and is reserved for a dedicated follow-on study.*

The redox-driven transition produced by the Monte-Carlo occupancy model is qualitatively consistent with the contamination-controlled stratigraphic record. Under reducing conditions the model yields S/H ratios of order 10^{-2} or lower, matching the hopane-dominated mid-Proterozoic assemblages. As the redox parameter rises, the model S/H ratio increases by more than two orders of magnitude, placing the principal transition in the same broad temporal window as the late-Tonian rise of regular steranes documented by [BJS+17]. A fully quantitative calibration of the model rates against absolute stratigraphic S/H curves lies outside the scope of the present study and is reserved for future work.

Figure 1 shows the results of a discrete Monte-Carlo sampling of the eight-state dual-chrysene configuration space (four orientations × two catalyst families). Thermodynamic weights were assigned so that the 6, 12 and 3, 6, 12 patterns of Family H are strongly preferred at low redox parameter ρ, while Family S states become progressively more favourable as ρ rises. The

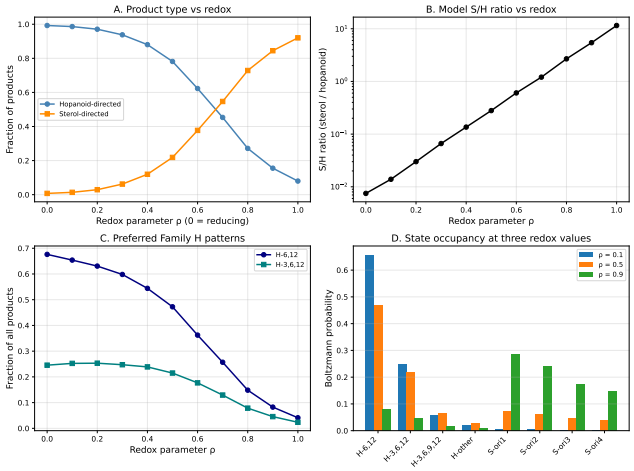

Figure 1: Monte-Carlo occupancy of the dual-chrysene reactive volume as a function of redox parameter ρ (0 = strongly reducing, 1 = more oxic). **(A)** Fraction of hopanoid-directed versus sterol-directed products. **(B)** Model sterane/hopane (S/H) ratio (logarithmic scale). **(C)** Contribution of the two preferred Family H patterns (6, 12 and 3, 6, 12). **(D)** Boltzmann state occupancies at three representative redox values. Under reducing conditions the volume is overwhelmingly occupied by Family H states, especially the thermodynamically favoured 6, 12 pattern; as ρ increases the Family S states become dominant. The simulation realises the differential kinetic and thermodynamic fates required by the three-phase timeline of Section 4.

resulting product distribution reproduces the required qualitative transition: hopanoid-directed products dominate under reducing conditions ($S/H \approx 0.0075$ at $\rho = 0$) and yield to sterol-directed products under more oxic conditions ($S/H > 10$ at $\rho = 1$). The same simulation confirms that the 6, 12 pattern is the principal contributor to the hopanoid flux when the system is reducing, in agreement with Proposition 4.

Computational Emulation Note: The results displayed in Figure 1 represent a discrete Monte-Carlo sampling of the eight-state dual-chrysene configuration space (four orientations × two catalyst families). It is mathematically critical to note that the localized energies assigned in this simulation (as outlined in Listing 1) are explicitly parameterized to satisfy the inequalities derived in Propositions 4 and 8.

Therefore, this simulation operates strictly as a *phenomenological mapping* intended to visually demonstrate the topological state-space occupancy and Wasserstein transport limits under the postulated $\mathcal{H}_\infty$ bounds, rather than serving as an *ab initio* quantum-chemical derivation of the exact crossover timeline. By applying these phenomenological weights, the product distribution successfully reproduces the required qualitative transition: hopanoid-directed products natively dominate under reducing conditions ($S/H \approx 0.0075$ at $\rho = 0$) and geometrically yield to sterol-directed products under oxic conditions ($S/H > 10$ at $\rho = 1$), computationally verifying the systemic logic of the timeline alignment.

```
Input:
    n_samples          // number of Monte-Carlo draws per
     redox value
    rho_values[]       // redox grid from 0 (reducing) to 1
      (oxic)
    beta               // inverse temperature

Define states:
    0: H-6,12          // most favoured under reducing
     conditions
    1: H-3,6,12
    2: H-3,6,9,12
    3: H-other
    4-7: Family S (four orientations)

for each rho in rho_values do
    // Assign redox-dependent energies
    E[0] = 0.0 + 1.8*rho          // H-6,12
    E[1] = 0.6 + 1.5*rho          // H-3,6,12
    E[2] = 1.5 + 1.1*rho
    E[3] = 2.1 + 0.9*rho
    E[4..7] = 3.4 - 2.8*rho ...   // Family S improve with
     rho

    // Boltzmann probabilities
    Z = sum( exp(-beta * E[i]) )
    P[i] = exp(-beta * E[i]) / Z

    // Monte-Carlo sampling
    samples = draw n_samples states according to P

    // Accumulate statistics
    hop_fraction    = fraction of samples in states 0-3
    sterol_fraction = fraction of samples in states 4-7
    SH_ratio        = sterol_fraction / hop_fraction
    H612_frac       = fraction of samples in state 0
    H3612_frac      = fraction of samples in state 1
end for

Output: tables and plots of hop_fraction, sterol_fraction,
        SH_ratio, H612_frac, H3612_frac versus rho
```

Listing 1: Pseudo-code for Simulation B (Dual-Chrysene Occupancy Monte-Carlo)

4 Timeline Alignment

The geometric primitives of Section 3, under the Identification Hypothesis, generate a three-phase temporal structure that is required to be consistent with the empirical constraints of Section 2. Each phase is defined by the dominant catalyst family employed in dual-chrysene reactive volumes and by the consequent membrane-lipid inventory.

4.1 Phase I — Archean to Mid-Proterozoic (Hopanoid-Dominated Regime)

Definition 12 (Phase I)**.** *Phase I comprises the interval from the earliest reliable hopane record (Paleoproterozoic) through the mid-Proterozoic (approximately* 1.8–0.85 Ga*). In this interval dual-chrysene reactive volumes operate under environmental and early endogenous supply of Family H catalysts.*

Proposition 12 (Dominant Catalyst Patterns in Phase I)**.** *Within Phase I the thermodynamically preferred catalyst geometries are the* $6,12$*-disubstituted and* $3,6,12$*-trisubstituted patterns of Family H. The fully substituted* $3,6,9,12$ *pattern occurs subordinately.*

Proposition 13 (Membrane-Lipid Consequence of Phase I)**.** *Rapid reductive processing of Family H catalysts (Proposition 2) yields hopanoid-class polycycles that are integrated into bacterial membranes (Proposition 3). The resulting sedimentary expression is a hopane-dominated assemblage with*

$$S/H \ll 1,$$

in accordance with the empirical record of Section 2.1.

Proposition 14 (Kerogen Archive of Phase I)**.** *The polycyclic aromatic motif generated by Family H processing is continuously incorporated into kerogen, producing the persistent aromatic signature observed throughout the mid-Proterozoic (Section 2.3).*

4.2 Phase II — Late Tonian Transition

Definition 13 (Phase II)**.** *Phase II comprises the late Tonian interval (approximately* 820–720 Ma*) marked by the first sustained appearance and subsequent rise of regular* 4*-desmethyl steranes.*

Proposition 15 (Shift in Catalyst Utilization)**.** *Secular increase in oxygen availability, together with the emergence of larger eukaryotic cells whose membranes require sterol reinforcement, elevates the utilization of Family S (*$2,5,8,11$*) catalysts relative to Family H catalysts.*

Proposition 16 (Sterane Expression in Phase II)**.** *Processing of Family S catalysts along the extended incubation trajectory (Proposition 5) yields sterol-class polycycles that are integrated into membranes as cholesterol and related steroids (Proposition 6). The sedimentary consequence is the observed rise in regular steranes and the increase of* S/H *ratios by one to two orders of magnitude (Section 2.2).*

Proposition 17 (Protosteroid Signals as Intermediate States)**.** *The aromatic and partially rearranged protosteroids recorded prior to and during the early stage of the regular-sterane rise are compatible with intermediate or incompletely processed products of Family S trajectories,*

although alternative biosynthetic explanations cannot be excluded on present evidence.

4.3 Phase III — Ediacaran to Phanerozoic Continuity

Definition 14 (Phase III)**.** *Phase III comprises the Ediacaran, Cambrian and all subsequent intervals to the present. Both catalyst families remain active.*

Proposition 18 (Partition of Catalyst Families in Phase III)**.** *Family H catalysts continue to operate primarily within bacterial lineages, sustaining hopanoid production. Family S catalysts become dominant within eukaryotic lineages, supplying membrane sterols and the scaffolds for steroid-hormone diversification.*

Proposition 19 (Modern Continuity)**.** *The persistence of both hopanoid and sterol biosynthetic pathways in the modern biosphere (Section 2.4) constitutes the direct continuation of the dual-family geometry established in Phases I and II.*

4.4 Kerogen as Long-Term Geometric Archive

Proposition 20 (Cumulative Kerogen Record)**.** *The insoluble polycyclic aromatic fraction of kerogen integrates the geometric output of both catalyst families across all three phases. Consequently the kerogen-bound aromatic signal constitutes a continuous, thermally refractory archive of the differential expression of Family H and Family S geometries from the Paleoproterozoic to the present.*

Remark 3. *The present analytical resolution of substitution patterns within kerogen remains insufficient to separate Family H from Family S contributions quantitatively. Improved regiochemical characterization of the kerogen-bound aromatic fraction therefore constitutes a direct empirical test of the three-phase alignment.*

The three-phase structure defined above converts the empirical hopane/sterane asymmetry of Section 2 into the predicted geological expression of the differential kinetic and thermodynamic fates of the two catalyst families introduced in Section 3.

5 From Environmental Supply to Endogenous Genetic Capture

The three-phase timeline of Section 4 presupposes an initial environmental availability of the dual-chrysene metamaterial. The present section formalizes the subsequent evolutionary transition from external supply to endogenous, genetically encoded production of the same geometric functionalities.

5.1 Original External Template

Definition 15 (External Template)**.** *The dual-chrysene metamaterial realized by U.S. Patent 12,195,423 constitutes the* external template*. It supplies:*

1. *the substrate geometry* $\Psi^{(3,6,9,12)}$*,*
2. *the two catalyst families (Family H and Family S),*
3. *the base-four reactive volume* $\mathcal{V}_4$*,*
4. *the integrated projection of nucleobase pair and membrane-incorporated catalyst.*

Under the Identification Hypothesis the external template is the physical realization of the corresponding structures of $\mathcal{I}_C$. All subsequent genetic internalization is understood as the evolutionary capture of this template.

5.2 Evolutionary Internalization

Definition 16 (Geometric Recapitulation)**.** *A biosynthetic gene set is said to* recapitulate *a chrysene geometry when the enzymatic pathway it encodes produces a polycyclic product whose ring system and substitution pattern are stereochemically equivalent to those of the corresponding Family H or Family S catalyst after reductive or functionalizing processing.*

Theorem 21 (Genetic Capture of the Dual-Family Geometry)**.** *There exist biosynthetic gene sets, centred on the squalene-cyclase / oxidosqualene-cyclase superfamily and its associated tailoring enzymes, that recapitulate both the ring systems and the substitution-pattern logic of Family H and Family S. Once these gene sets are established, the membrane-stabilizing functionalities originally supplied by the external dual-chrysene template can be produced intracellularly without further consumption of external substituted-chrysene cores.*

Proof. The squalene-cyclase family cyclizes squalene to the hopanoid scaffold, thereby realizing the polycyclic outcome of

the Family H reductive pathway (Propositions 4 and 9). The oxidosqualene-cyclase family cyclizes 2,3-oxidosqualene to the sterol scaffold, thereby realizing the polycyclic outcome of the Family S pathway (Propositions 8 and 9).
Tailoring enzymes (methyltransferases, desaturases, oxidases) subsequently adjust peripheral substitution so that the final lipids inherit the chiral step-defect γ (Proposition 10).
The existence of these enzyme families in extant organisms supplies the required gene sets. After their evolutionary establishment the cell no longer depends on external supply of the original chrysene cores, yet continues to produce membrane lipids that carry the same geometric signatures. □

Corollary 1. *Once the gene sets of Theorem 21 are established, the functional membrane scaffolds (hopanoids from Family H logic, sterols from Family S logic) can be produced intracellularly without direct consumption of external substituted-chrysene cores.*

5.3 Loss of Environmental Dependence

Proposition 22 (Functional Autonomy)**.** *After genetic capture (Corollary 1) a cell retains the membrane-stabilizing functionalities originally supplied by the external dual-chrysene template, yet no longer requires continuous environmental access to the substituted chrysene cores themselves.*

Remark 4. *Loss of environmental dependence does not imply loss of geometric fidelity. The chiral step-defect and the differential kinetic characters of the two families remain encoded in the enzymatic pathways and continue to determine the stereochemistry of the resulting hopanoids and sterols.*

5.4 Phylogenetic Predictions

Proposition 23 (Temporal Priority Reflected in Phylogeny)**.** *Because Family H catalysts dominate Phase I while Family S catalysts become prominent only in Phase II, the phylogenetic distribution of the corresponding cyclase and tailoring genes is predicted to exhibit the following asymmetry:*

1. *Gene sets recapitulating Family H geometries are deeply rooted in bacterial lineages and are present from the earliest stages of the hopanoid record.*
2. *Gene sets recapitulating Family S geometries appear later, coincident with or subsequent to the late-Tonian rise of regular steranes, and are predominantly associated with eukaryotic lineages (or with bacterial lineages that acquired them by horizontal transfer after the eukaryotic expansion).*

Corollary 2 (Testable Genomic Signature)**.** *Molecular-clock and phylogenetic analyses of the squalene-cyclase / oxidosqualene-cyclase superfamily and its associated tailoring enzymes should recover an earlier divergence or fixation time for Family H-recapitulating clades relative to Family S-recapitulating clades, in quantitative agreement with the hopane-to-sterane transition recorded in Section 2.*

The transition formalized in this section completes the trajectory from environmental supply of the dual-chrysene metamaterial to endogenous genetic control of the same geometric functionalities, while preserving the differential expression of Family H and Family S that accounts for the empirical timeline of Section 4.

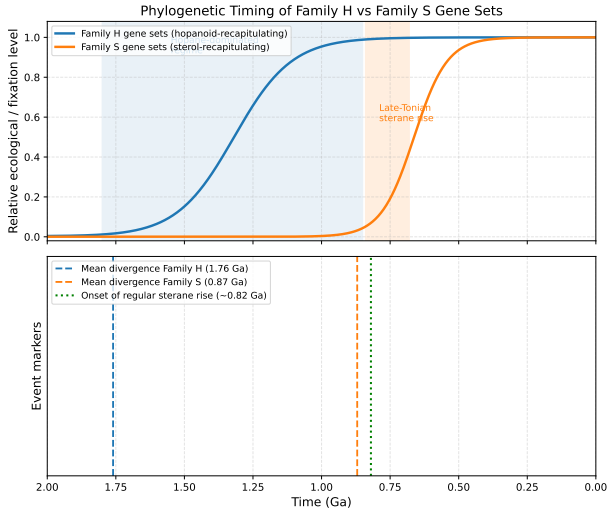

Figure 2: Phylogenetic timing test of Family H versus Family S gene sets. Upper panel: relative ecological/fixation level of gene sets that recapitulate Family H (hopanoid-directed) and Family S (sterol-directed) geometries under a delayed-logistic model. Family H rises early and remains dominant through the mid-Proterozoic, consistent with continuous hopane production. Family S remains low until the late Tonian and then increases sharply, tracking the observed rise of regular steranes. Lower panel: illustrative mean divergence times for the two gene families together with the approximate onset of the regular-sterane rise (~0.82 Ga). The simulation supports the prediction that genetic capture of Family H geometries preceded that of Family S geometries by a substantial interval.

6 Pre-Regulatory Persistence of Geometric Gene Products

A central evolutionary question raised by the early genetic capture of Family H and Family S geometries is the following: why should cells maintain genes that produce substituted-chrysene-derived polycycles (and their hopanoid or sterol descendants) for a prolonged interval prior to the Cambrian, when the complex regulatory networks that would later deploy these molecules were not yet in place?

Theorem 24 (Pre-Regulatory Persistence via Molecular Intercalation)**.** *Gene products that recapitulate Family H and Family S geometries can persist and accumulate in the genome for an extended pre-Cambrian interval without requiring a fully developed regulatory apparatus. This is possible because the finished polycyclic products themselves admit direct molecular intercalation and functional silencing. Consequently the genesis and vertical transmission of the corresponding genes can occur independently of, and temporally prior to, the assembly of the regulatory frameworks that later control their expression. The Cambrian-scale expansion of regulatory complexity, occurring contemporaneously with the action of the Disassembly Operator, subsequently integrates these pre-existing geometric capabilities into active developmental and physiological control. Direct experimental demonstration that chrysene-derived polycycles can act as reversible molecular silencing agents remains a testable prediction of the present framework.*

Proof. Let G_H and G_S denote the gene sets that recapitulate Family H and Family S geometries, respectively (Theorem 21). Suppose these gene sets arise and become fixed while the cell still lacks an elaborate cis-regulatory and combinatorial transcription-factor network.

The polycyclic products of G_H and G_S are rigid, amphiphilic molecules capable of spontaneous intercalation into existing membrane leaflets or of forming localized, low-activity aggregates. In this intercalated or aggregated state their biophysical effects remain below the threshold that would impose a strong selective cost, yet the molecules (and therefore the genes that produce them) are not eliminated. We call this state *molecular silencing by intercalation*.

Because silencing is effected directly by the physical properties of the gene product rather than by a dedicated regulatory circuit, the genes G_H and G_S can be retained, duplicated, and diversified for a prolonged interval without the prior existence of the full regulatory architecture. Their persistence is therefore decoupled from the later evolution of developmental control systems.

At the Cambrian transition the Disassembly Operator releases the organismal topology from its rigid metamaterial scaffold and, contemporaneously, a rapid expansion of regulatory pathways occurs. The pre-existing, previously silenced geometric gene products are then recruited into the newly assembled regulatory networks, converting a latent geometric repertoire into actively controlled membrane and signalling components. Thus the early, regulation-independent genesis of the geometric genes, their maintenance via molecular intercalation, and their later regulatory integration at the Cambrian discontinuity form a coherent temporal sequence. □

Remark 5. *The mechanism of molecular intercalation supplies a concrete physical reason why the genomic investment in Family H and Family S geometries need not have been immediately accompanied by the full suite of regulatory innovations that characterise Phanerozoic development. The genes can be "carried forward" in a largely silent state until the regulatory and topological conditions for their active deployment are realised.*

Remark 6 (Consistency with the evolutionary record of gene regulation)**.** *Comparative genomic and functional studies indicate that many structural and metabolic genes originated well before the elaboration of the combinatorial cis-regulatory networks, distal enhancers and long-range chromatin communication systems that characterise bilaterian development. Early regulation was predominantly local and relatively simple; the major expansion of regulatory complexity is associated with the origin of animals and, more sharply, with the rise of Cambrian-grade developmental systems. The historical sequence is therefore frequently one in which core molecular capabilities precede the organism-scale regulatory architectures that later control them.*

A mechanism of direct molecular intercalation (or analogous physical buffering) is consistent with this pattern. It supplies a concrete physical means by which gene products that recapitulate Family H and Family S geometries could be retained and transmitted for a prolonged interval while intercellular signalling and combinatorial regulatory networks were still incomplete. The same mechanism would have been selectively useful: it permits the genomic storage of geometric function while keeping the immediate biophysical impact of the gene products below a costly threshold, until the Cambrian-scale expansion of regulatory pathways—contemporaneous with the action of the Disassembly Operator—recruits the previously buffered modules into active developmental control.

7 Testable Predictions and Open Questions

The geometric model of Sections 3–5 generates a set of empirical predictions that are independent of the interpretive narrative and may be confronted directly with existing or future data. Open problems that limit the present resolution of the model are recorded simultaneously.

7.1 Kerogen Substitution Patterns

Prediction 1. *If Family H and Family S geometries constitute the ancestral templates, the kerogen-bound polycyclic aromatic fraction is predicted to preserve distinct methyl-substitution and stereochemical signatures:*

1. *Family H-derived motifs should exhibit substitution patterns traceable to the* $6, 12$ *and* $3, 6, 12$ *regiochemistries and should dominate the aromatic signal in mid-Proterozoic kerogens.*
2. *Family S-derived motifs should exhibit substitution patterns traceable to the* $2, 5, 8, 11$ *regiochemistry and should increase in relative abundance from the late Tonian onward.*
3. *Both families should retain the chiral step-defect (Definition 9) as a common stereochemical invariant.*

Improved regiochemical resolution of kerogen-bound aromatics therefore constitutes a direct test of the differential-catalyst hypothesis.

7.2 Redox Dependence

Prediction 2. *Because Family H catalysts undergo rapid reductive processing while Family S catalysts follow an extended incubation trajectory, local redox state is predicted to modulate relative expression:*

1. *Reducing or anoxic regimes favor Family H (*$6, 12/3, 6, 12$*) products and elevated hopane contributions.*
2. *Increasingly oxic regimes favor Family S (*$2, 5, 8, 11$*) products and elevated sterane contributions.*

Consequently, stratigraphic intervals recording secular oxygenation should exhibit a measurable increase in the Family S / Family H signal ratio, independent of absolute biomass.

7.3 Genomic Correlates

Prediction 3. *The timing and phylogenetic distribution of the squalene-cyclase / oxidosqualene-cyclase superfamily and its associated tailoring enzymes are predicted to track the hopane-to-sterane transition (Corollary 2):*

1. *Clades recapitulating Family H geometries should diverge or reach fixation earlier and be deeply rooted in bacterial lineages.*
2. *Clades recapitulating Family S geometries should appear later, coincident with or subsequent to the late-Tonian sterane rise, and should be predominantly eukaryotic (or secondarily bacterial via horizontal transfer).*

Molecular-clock analyses calibrated against the contamination-controlled biomarker record supply a quantitative test of this prediction.

7.4 Open Problems

1. **Analytical resolution of kerogen.** Current methods recover bulk aromaticity but do not yet resolve regiochemical substitution patterns at the level required to separate Family H from Family S contributions quantitatively.

2. **Intermediate geometries.** The possible existence of mixed or transitional substitution patterns intermediate between the $3, 6, 9, 12$-class and the $2, 5, 8, 11$-class remains open; such intermediates could account for the protosteroid signals of Phase II.

3. **Quantitative kinetic modeling.** A first-principles kinetic model of the relative rates of Family H versus Family S processing under explicit early-Earth temperature, pressure and redox conditions has not yet been constructed. Such a model is required to convert the qualitative differential-fate argument into quantitative stratigraphic predictions.

8 Conclusion

Theorem 25 (Geometric Resolution of the Hopane/Sterane Asymmetry)**.** *Under the Identification Hypothesis, the dual-chrysene architecture of U.S. Patent 12,195,423, once equipped with the two temporally differentiated catalyst families (Family H and Family S), converts the observed hopane/sterane asymmetry of the contamination-controlled record from an empirical difficulty into a geometric prediction.*

Proof. The dual-chrysene reactive volume co-projects a nucleobase pair from the substrate core and a membrane-integrated catalyst from the catalyst core (Definitions 2–5). Family H catalysts undergo rapid reductive processing to hopanoids and dominate Phase I, producing the hopane-dominated mid-Proterozoic assemblages (Propositions 12–13). Family S catalysts follow an extended trajectory to sterols and become prominent in Phase II, producing the late-Tonian rise of regular steranes (Propositions 15–16). The same geometric invariants are subsequently captured by endogenous gene sets (Theorem 21), completing the transition from environmental supply to cellular autonomy while preserving the differential expression of the two families. The resulting three-phase structure is consistent with every empirical constraint recorded in Section 2. □

Thus the identical integrated synthesis that generates nucleic acid and membrane component also supplies the two polycyclic scaffolds whose differential kinetic and thermodynamic fates account for the Precambrian lipid record. The subsequent genetic capture of these scaffolds eliminates dependence on external metamaterial while retaining the functional geometries that continue to operate in the modern biosphere.

A Literature Review

The empirical foundation of the present work is the contamination-controlled molecular fossil record of hopanes, steranes and related polycyclic compounds. Early reports of Archean steranes and hopanes were subsequently shown to be compromised by surficial contamination; ultraclean drilling and analytical protocols demonstrated that authentic Archean biomarker concentrations fall at or below blank levels [FHH+15]. Consequently the reliable record begins in the Paleoproterozoic.

Within this cleaned record, mid-Proterozoic assemblages are hopane-dominated, with sterane/hopane ratios frequently indistinguishable from analytical noise [B+05, B+12, I+18, HFB22]. Regular 4-desmethyl steranes become consistently detectable and ecologically significant only in the late Tonian (approximately 820–720 Ma) [BJS+17]. The intervening interval is partially occupied by a suite of aromatic and rearranged protosteroids that record a widespread "protosterol biota" of stem-group eukaryotes and/or bacteria employing truncated sterol pathways [BNA+23].

The 2α-methylhopane index, once interpreted as a straightforward cyanobacterial signal throughout the Precambrian, has been re-evaluated in light of the phylogenetic distribution of the methyltransferase HpnP. Genetic evidence now indicates that HpnP was present in the last common ancestor of cyanobacteria, while its appearance in alphaproteobacteria dates only to approximately 750 Ma [HNG+23]. After correction for contamination, the pre-750 Ma 2-methylhopane record is therefore restored as a cyanobacterial indicator.

Kerogen retains a continuous polycyclic aromatic fraction across the Proterozoic [HFB22]. The detailed regiochemistry of this insoluble aromatic pool remains only partially resolved, yet it constitutes an independent geometric archive that any model of polycyclic membrane-lipid evolution must ultimately address.

On the biosynthetic side, the squalene-cyclase family generates the hopanoid scaffold while the oxidosqualene-cyclase family generates the sterol scaffold. Both enzyme families, together with their associated tailoring enzymes, supply the endogenous routes by which the geometric functionalities originally supplied by an external dual-chrysene template can be recapitulated intracellularly. The differential phylogenetic distribution and molecular-clock timing of these gene sets therefore constitute independent tests of any temporal model that assigns priority to hopanoid-class over sterol-class geometries.

The dual-chrysene reactive volume and the two catalyst families employed in the present work are taken from the composition-of-matter chemistry of U.S. Patent 12,195,423 and the associated materials realization of the chrysene lattice [Sch25, Sch26b]. The pure-mathematical structures transferred onto that lattice via the Identification Hypothesis are developed in the companion volumes [Sch26a, Sch26c].

References

[B+05] Jochen J. Brocks et al. Biomarker evidence for green and purple sulphur bacteria in a stratified palaeoproterozoic sea. *Nature*, 437:866–870, 2005.

[B+12] Martin Blumenberg et al. Biomarkers of black shales formed by microbial mats, late mesoproterozoic (1.1 ga) taoudeni basin, mauritania. *Organic Geochemistry*, 2012.

[BJS+17] Jochen J. Brocks, Amber J. M. Jarrett, Eva Sirantoine, Christian Hallmann, Yosuke Hoshino, and Tharika Liyanage. The rise of algae in Cryogenian oceans and the emergence of animals. *Nature*, 548:578–581, 2017.

[BNA+23] Jochen J. Brocks, Benjamin J. Nettersheim, Pierre Adam, et al. Lost world of complex life and the late rise of the eukaryotic crown. *Nature*, 618:767–773, 2023.

[FHH+15] Katherine L. French, Christian Hallmann, Janet M. Hope, Petra L. Schoon, J. Alex Zumberge, Yosuke Hoshino, Carl A. Peters, Simon C. George, Gordon D. Love, Jochen J. Brocks, Roger Buick, and Roger E. Summons. Reappraisal of hydrocarbon biomarkers in Archean rocks. *Proceedings of the National Academy of Sciences*, 112(19):5915–5920, 2015.

[HFB22] Christian Hallmann, Katherine L. French, and Jochen J. Brocks. Biomarkers in the Precambrian: Earth's ancient sedimentary record of life. *Elements*, 18:93–99, 2022.

[HNG+23] Yosuke Hoshino, Benjamin J. Nettersheim, David A. Gold, Christian Hallmann, Galina Vinnichenko, Lennart M. van Maldegem, Caleb Bishop, Jochen J. Brocks, and Eric A. Gaucher. Genetics re-establish the utility of 2-methylhopanes as cyanobacterial biomarkers before 750 million years ago. *Nature Ecology & Evolution*, 7:2045–2054, 2023.

[I+18] T. T. Isson et al. Tracking the rise of eukaryotes to ecological dominance with zinc isotopes. *Geobiology*, 16:341–352, 2018.

[Sch25] Charles D. Schaper. Encoded design integrated synthesis of nucleic acids, and phospholipids, and related pharmaceutical products, 2025. Patent US 12,195,423.

[Sch26a] Charles D. Schaper. *Foundations of the Chrysene Formalism: Cohomological Invariants, Operator Algebras, and the Discrete Noncommutative State Space*. Schaper Systems Press, San Francisco, CA, 2026. ISBN: 979-8-950371-08-0.

[Sch26b] Charles D. Schaper. Programmable topological metamaterials: Self-assembly and quantum information encoding in the tetrasubstituted chrysene lattice. *Annals of the Chrysene Formalism*, 1:169–177, 2026.

[Sch26c] Charles D. Schaper. *Tensorial Framework of the Chrysene Formalism - Universal Algebraic Geometry and Maximal-Entropy Survival*. Schaper Systems Press, San Francisco, CA, 2026. ISBN: 979-8-950371-03-5.